Measuring Atmospheric Icing Rate in Mixed-Phase Clouds Using Filtered Particle Data

Eero O. Molkoselkä, Ville A. Kaikkonen, and Anssi J. Mäkynen

***Abstract*—In-cloud icing of objects is caused by super-cooled microscopic water droplets carried by the wind. To estimate the icing rate of objects in such conditions, the liquid water content (LWC) of the icing cloud and the median volume diameter (MVD) of the droplets are measured. Mixed-phase clouds also contain ice crystals which must be ruled out in order to avoid overestimation of the icing rate. Typically, cloud droplet instruments are not able to do this. A particle imaging instrument ICEMET (icing condition evaluation method) was used to observe in-cloud icing conditions. This lensless device uses a computational imaging method to reconstruct the shadow images of the microscopic objects. The size, position and shape descriptors of each particle are measured. This data is then used to filter out the ice crystals. The droplet size distribution and the size of the measurement volume are used to determine the LWC and MVD. The performance of the instrument was tested under mixed-phase icing conditions in a wind tunnel and on a wind turbine. The measured LWC and MVD values were used to model the ice accretion on a cylinder-shaped object according to ISO 12494:2017 icing standard. In the wind tunnel, the modeled ice mass was compared to the weighed ice mass collected by a cylinder. According to our results, ice accretion rates were overestimeted by 65.6 % on average without filtering out the ice crystals. Thus, the ability to distinguish between droplets and ice crystals is essential for estimating the icing rate properly.**

***Index Terms*—Atmospheric measurements, cloud droplets, digital holography, ice accretion, ice crystals, icing, image analysis, LWC, MVD**

I. Introduction

Atmospheric in-cloud icing of structures is a common challenge in cold regions. The phenomenon is caused by super-cooled cloud droplets that freeze on surfaces forming a layer of ice. When left unnoted, the ice load can build up for long periods eventually damaging the structure. Traditionally, overhead power lines and towers have had the most issues because of in-cloud icing [1]. However, as wind power has gained more popularity, it has become clear that icing also has a negative impact on wind energy production. Even a small ice accretion on turbine blades is enough to alter its aerodynamic properties and result in the loss of power production. Higher ice loads cause mass imbalance and high amplitude vibrations which can eventually damage the turbine [2]. This creates a demand to monitor and be able to predict in-cloud icing events in real time.

The ice accretion rate depends on multiple environmental factors, such as particle concentration of the air, wind speed and the surface properties of the structure [1]. In case of cloud droplets, liquid water content (LWC) is used to measure the mass of liquid water in a cubic meter of air. The icing rate also depends on the size of the droplets in relation to the size of the icing object as it affects the collision efficiency of the droplets. In-cloud icing is mainly caused by droplets with a diameter of 10 to 30 microns [3], [4]. For droplets, the median volume diameter (MVD) can be used to approximate the size distribution by using a single number [5]. It refers to the point in droplet size distribution (DSD) where the cumulative water mass is half of the total water mass. Close to the ground level LWC and MVD are heavily dependent on the local geographical factors and, *in situ* measurements are required to obtain accurate data [1], [6].

Icing clouds are often the so called mixed-phase clouds which contain both liquid water droplets and ice crystals. Typically, the most of the icing models ignore the ice crystals as in the conditions near the ground level their concentration is not very high [6]. In addition, accurate shape information is required in order to correctly calculate their mass. Cloud droplets can be considered as spherical which simplifies their volume approximation. Ice crystals on the other hand form different types of complex shapes [7]. With common icing measurement techniques, the shape retrieval is nearly impossible. Most of the methods commonly used cannot differentiate between ice crystals and droplets.

ISO 12494:2017 icing standard describes a method for measuring ice accretion by using a rotating cylinder with a diameter of 30 mm and minimum length of 0.5 m [8]. The ice accretion is typically measured by weighing the cylinder either manually or automatically.

Several light scattering based instruments have been developed to measure the cloud properties [9], [10]. The method works by focusing a laser beam on a small volume and measuring intensity changes caused by crossing objects. One drawback with this method is that typically the size of the sampling volume depends on the speed of the airflow. This means that accurate wind speed information is required. The method also has drawbacks when it comes to mixed-phase conditions. For example, a commercially available light scattering based instrument CDP-2 (Cloud

This work was supported in part by European Regional Development Fund (ERDF) under European Territorial Cooperation (ETC) program Interreg V A Nord through Grant NYPS 20202472 and in part by Regional Council of Lapland through Grant 126/00.01.05.24.02/2019.

Droplet Probe) is not capable of differentiating between droplets and small ice crystals [10].

Digital holography and other image based instruments have gained more popularity in the last decade [11]–[16]. The holographic method allows the computational reconstruction of the shadow images of the objects inside the measurement volume. The individual particles can then be analyzed one at the time. The 3D position, shape and size information about the particles can be obtained. One of the method's advantages in cloud droplet imaging is that the measurement volume is constant and not wind speed dependent.

In this study we present a digital holography based particle imaging method that is capable of measuring LWC and MVD values in mixed-phase clouds and filtering out ice crystals. We also show proof that the filtering is necessary for modeling ice accretion accurately. This paper is an extension to the I²MTC 2020 proceedings paper titled *Instrument and Method for Measuring Ice Accretion in Mixed-Phase Cloud Conditions* [17].

II. Materials and Methods

A. Estimating Ice Accretion

The icing standard provides a model for estimating the ice accretion of several types of structures, such as masts, towers and cables [8]. According to the standard the icing rate d_m/d_t (g/s) can be obtained using (1).

$$d_m/d_t = \eta_1\eta_2\eta_3 \cdot w \cdot A \cdot v \tag{1}$$

The parameter w is the mass concentration of the particles, A is the cross-sectional area of the icing object and v is the velocity of the particles. For cloud droplets, w is equal to the LWC and v is typically assumed to be equal to the wind speed for stationary structures. η_{1-3} are collision, sticking and accretion factors varying between 0–1. They represent the portions of particles that do not flow past, bounce off or melt away from the object. During in-cloud icing conditions η_2 and η_3 are typically assumed to be 1 for cloud droplets. However, η_3 can be lower than 1 if the droplets are large enough or the temperature is close to 0 °C [8].

The standard includes a model for approximating the collision factor η_1 for cloud droplets and a cylinder shaped icing object. The model uses parameters K and ϕ which are be obtained with (2) and (3).

$$K = \rho_w d^2/(9\mu D) \tag{2}$$

$$\phi = Re^2/K \tag{3}$$

The parameter ρ_w is the water density, d the droplet diameter (MVD), μ the absolute viscosity of the air, D the icing cylinder diameter and Re is the droplet Reynolds number. Re can be calculated with (4) where ρ_a is the air density and v the particle velocity.

$$Re = \rho_a dv/\mu \tag{4}$$

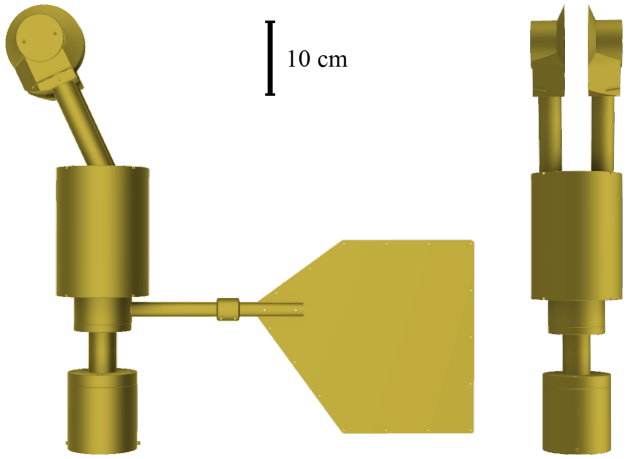

Fig. 1. ICEMET-sensor 3D rendering from side (left) and front (right).

Finally, η_1 can be modeled by using K and ϕ (5).

$$\begin{aligned} \eta_1 &= A\text{–}0.028\text{–}C(B\text{–}0.0454) \\ A &= 1.066K^{-0.00616}exp(-1.103K^{-0.688}) \\ B &= 3.641K^{-0.498}exp(-1.497K^{-0.694}) \\ C &= 0.00637(\phi - 100)^{0.381} \end{aligned} \tag{5}$$

LWC and MVD are typically considered as the two most challenging parameters of the model to measure in field conditions [1], [3], [5]. In order to accurately measure the liquid water content and droplet sizes, a sufficient volume of the air has to be sampled and the droplets in the volume measured. Ideally, the droplets should be separated from unwanted particles such as ice crystals.

A simple method for modeling wind turbine blade ice accretion based on the icing cylinder modeling has been proposed [18]. In these simulations, the ice accretion per meter on the NREL 5 MW reference turbine blade was 20 times higher on average than the accretion on the ISO 12494:2017 cylinder. The reported wind speed was 7.5 m/s, temperature -5 °C, droplet size 25 µm, LWC 0.2 g/m^3 and air pressure 96 kPa. However, different parameters were also tested. The rotational speed of the turbine was 12.4 RPM and the simulation length 60 minutes [18].

B. ICEMET System

The ICEMET-sensor (Fig. 1) is a novel holographic cloud droplet and particle imaging instrument [14], [15]. It is capable of measuring objects captured in the hologram from 5 µm up to 1 mm. This means that the sensor can measure the 10-30 µm diameter cloud droplets that typically cause icing of structures [3], [4]. The ICEMET-sensor is designed for *in situ* measurements in harsh icing conditions. The device has 500 W heating capacity to protect it from icing and it rotates freely to align itself correctly according to the wind direction. The sampling volume is bounded by two sharp disks which improves the aerodynamic properties of the sensor at different wind speeds [15], [19].

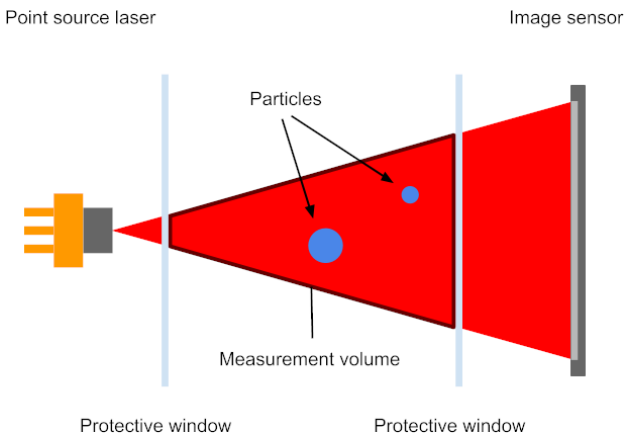

Fig. 2. The in-line holographic setup of the ICEMET-sensor. The distance between protective windows is 30 mm.

The in-line holographic setup of the ICEMET-sensor is shown in Fig. 2 [20]. Unlike most other holographic instruments, the laser beam is not collimated but acts as a point source. This reduces the cost and amount of optical elements needed in the system. The image sensor used is a grayscale Sony IMX264 with resolution of 2448x2048 pixels and pixel size of 3.45 µm. The laser is a 660 nm wavelength diode from Ushio Opto Semiconductors Inc. The setup forms a cone shaped 0.5 cm^3 measurement volume between the protective windows. The frame rate of the system is 6 images per second.

The point source setup of the sensor creates an optical magnification effect; the objects further from the image sensor appear larger. Their intensity is also lower because the light scatters to wider area. The optical magnification M changes linearly as a function of the object position along the z-axis and can be obtained with (6).

$$M(z) = z_{tot}/(z_{tot} - z) \tag{6}$$

The parameter z is the object position and z_{tot} is the distance between the sensor and the laser source.

The reconstruction of digital holograms is typically a computationally expensive task because the images often have a high resolution and large depth of the field. However, with modern hardware and proper parallel computing methods, it is possible to achieve real time performance. Today, this can be done with an ordinary desktop computer using almost any commercially available GPU (graphics processing unit).

We developed an image processing and particle analysis software called ICEMET-Server [21]. The software is built with modern C++ using OpenCV library and it is heavily multi-threaded and GPU accelerated [22]. Most of the algorithms developed are based on the ideas described by Fugal et al. [23].

C. Image Processing

The digital hologram processing pipeline of ICEMET-Server is presented in Fig. 3. The raw holograms are preprocessed by center cropping them to a resolution of 2048x2048 pixels to remove the lower intensity image edges and to provide more uniform lighting across the hologram. Background subtraction is used to reduce the unwanted noise and further equalize the illumination of the hologram. The image is divided by a background image and multiplied by its own mean pixel value. The background image is generated by taking the pixel-by-pixel median from a stack of seven consecutive holograms. The stack is updated every time a new hologram is captured, which dynamically changes the background image over the time.

The preprocessed digital holograms are reconstructed using angular spectrum propagation. The frequency domain filter H is applied to reconstruct the hologram to distance z (7).

$$H(u, v, z) = exp(-jkz\sqrt{1 - (\lambda u)^2 - (\lambda v)^2}) \tag{7}$$

The variables u and v are the distances from the center of the image, λ is the wavelength of the laser, j the imaginary unit and k the wavenumber [24]. The whole 30 mm sampling depth is reconstructed into a stack of 1500 images. Simultaneously, a new same sized image containing the minimum pixel values found in the whole stack for each pixel is created. The minimum image is formed by first selecting the first reconstructed hologram slice as the minimum image. Then the pixel values of the next reconstructed hologram slice are compared with each other and the lower values are chosen as the new minimum image pixel values. The result will be an image containing all the lowest and thus darkest values for each pixel. Because the shadow images of the objects appear darker than the background, they will all show in the minimum image. The 2D coordinates and approximate sizes of the objects can be found by binarizing the minimum image and using basic object detection. ICEMET-Server does this with OpenCV function *findContours* [22]. The information is used to create a rectangular 2D segment for each object.

The z-position of an object can be found by sliding the 2D segment through the reconstructed stack. The focusing can be automated by calling a scoring function at each z-position. The process is often called autofocusing. An ideal scoring function has its global maximum at the z-position of the object and no local peaks. Many different functions have been proposed for autofocusing [24]–[26]. Through a testing process, two different scoring functions were chosen. For objects with width and height smaller than 5 pixels, the minimum intensity of the segment is used. The method chooses the z-position with the lowest pixel value. The minimum based autofocusing is fast and because most of the objects found will be small droplets, the processing times will be reduced significantly. However, the function will not be able to correctly score larger objects with more complex shapes. For them, the maximum standard deviation of standard deviation filtered (SDoSDF) segment is used. The method applies a 3x3 standard deviation filter on the segment at every z-position and calculates the standard deviations

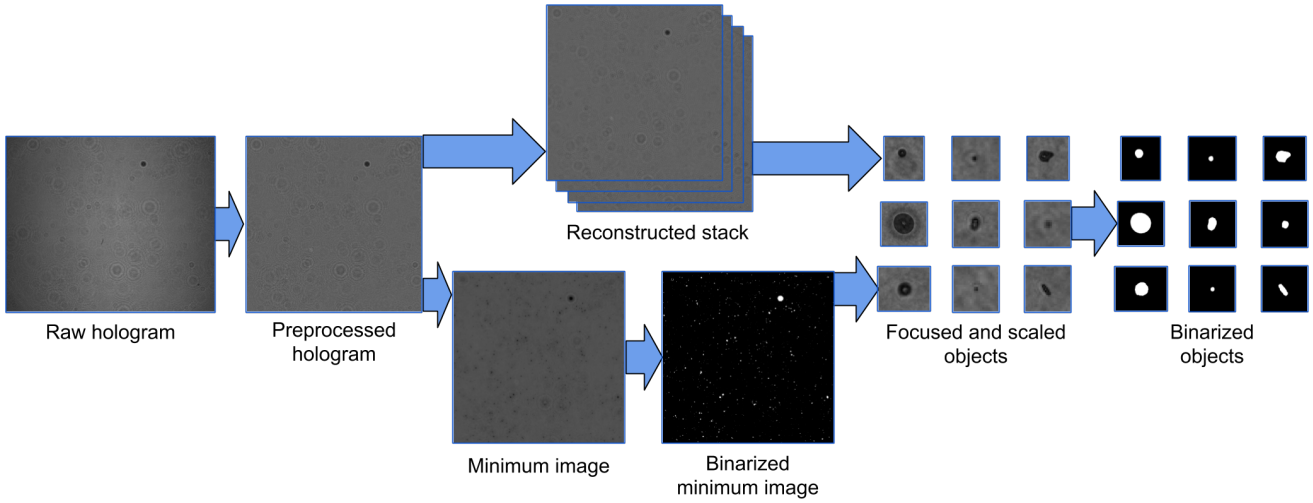

Fig. 3. ICEMET-Server hologram processing pipeline. First the raw hologram is cropped and background subtracted. Next the preprocessed image is reconstructed into a stack and minimum image. The xy-coordinates of individual objects are extracted from the binarized minimum image. The z-position is autofocused from the stack. Finally, the found objects are scaled and binarized.

of the filtered segments [27]. This method was found by experimenting with different autofocus functions. Many methods gave good results when used with snowflakes and other complex shapes but SDoSDF performed the best for circular droplets. To further accelerate the focusing process, a ternary search based greedy search algorithm is used to find the best score [28]. The method reduces the execution time approximately 90 % in comparison to iterating through the whole stack.

D. Analysis and Statistics

The perimeter calculation function of OpenCV uses pixel centroids [22]. This makes the comparison of objects with different sizes difficult as the perimeters of smaller objects will be relatively more underestimated. The focused object segments are scaled approximately to 200 pixels using Lanczos resampling [29]. This way the segment sizes will be almost the same throughout the analysis. For the smaller objects, the upscaling brings up their sub-pixel features that makes determining their shape more feasible (Fig. 4).

The scaled particles are binarized using a threshold I_{th} (8).

$$I_{th} = I_{bg} - 0.35(I_{bg} - I_{min}) \tag{8}$$

I_{bg} is the global background and I_{min} the local minimum of the segment. I_{bg} is calculated by taking the median of the preprocessed hologram. The constant 0.35 was chosen through a calibration process with NIST traceable microspheres [15]. The equivalent diameter is calculated using the area of the object. The perimeter p is also extracted and used to together with the equivalent diameter to obtain object's circularity factor f_c (9). The circularity factor is the real perimeter of an object divided by the perimeter derived from its area A when the object is assumed to be a circle.

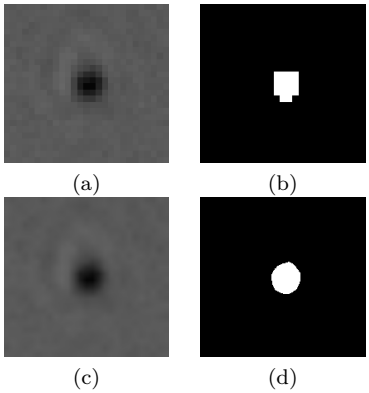

Fig. 4. (a) Original particle image (27x26 px). (b) Binarized particle image (27x26 px). (c) Upscaled particle image (200x193 px). (d) Upscaled and then binarized particle image (200x193 px).

$$f_c = p/(2\sqrt{\pi A}) \tag{9}$$

A lower value means that the object is more circular. The factor can be used to distinguish circular droplets from unwanted objects. All the droplet diameters are inserted into DSD bins.

Total water mass of the droplets is obtained by using their equivalent diameters and assuming that they are spherical. Because the sampling volume at every frame and the frame rate of the sensor are constant, total volume of the measurement can be calculated by multiplying the volume of a single frame by the number of frames. LWC is obtained by dividing the total water mass in all frames with the total volume of the measurement. MVD is calculated from the DSD [5].

E. Icing Measurements

Two measurement campaigns are presented: icing wind tunnel and wind turbine nacelle measurements. The wind tunnel measurements were done in the VTT icing wind

Fig. 5. The ICEMET-sensor and 0.5 m long standard cylinder in the VTT icing wind tunnel 2.0.

Fig. 6. The ICEMET-sensor on a wind turbine nacelle during winter 2016–2017.

TABLE I
WIND TUNNEL MEASUREMENT CONDITIONS

#	Temp. (°C)	Wind speed (m/s)	LWC (g/m^3)[a]
1	-5	7	0.2
2	-5	7	0.4
3a	-15	7	0.2
3b	-15	7	0.2
4	-15	10	0.2
5a	-15	7	0.4
5b	-15	7	0.4
6	-15	10	0.4
7	-15	20	0.4

[a] LWC value targeted by VTT wind tunnel operators.

tunnel 2.0 located in Espoo, Finland, in October 2016 [30]. The ICEMET-sensor was placed side by side with a rotating 0.5 m long standard cylinder as seen in Fig. 5. [8]. The accreted ice was weighed and removed after every measurement.

All the measurements and targeted conditions are presented in Table I. The parameters were temperature, wind speed and targeted LWC. The targeted LWC values were set by the wind tunnel operators by measuring and adjusting the water flow. The measurements #3a–b and #5a–b were made in the same conditions. The measurement durations were between 10 and 24 minutes.

After the wind tunnel measurements, the ICEMET-sensor was installed in a wind turbine nacelle in northern Finland (Fig. 6). The sensor measured natural icing conditions during the winter 2016–2017. The measurements were done in 1 minute bursts every 3 minutes.

The turbine installation did not include the icing standard cylinder measurements as a reference point and we were not able to measure the real weight of the accreted ice on the turbine blades. The measurement works as a demonstration of modeling a real world icing event.

III. Results

A. The Icing Wind Tunnel

The ICEMET-sensor's particle image data was analyzed with and without circularity factor filtering. With filtering enabled, all the particles with $f_c > 1.07$ were pruned. The threshold was chosen by using the particle data obtained from the wind tunnel measurement #1. The 700 000 particle images of the measurement were ordered by the f_c parameter and the initial threshold was selected by visual inspection where the droplets and ice crystals started to get mixed up with each other. After this the value was adjusted to match up with the targeted LWC of the measurement #1. The final threshold $f_c > 1.07$ has approximately ± 0.01 uncertainty.

The measurement results and the corresponding calculations are presented in Fig. 7 The targeted LWC values were compared with the values measured with the ICEMET-sensor. The MVD values measured with the ICEMET-sensor with both the filtered and unfiltered data are shown in Fig. 7 (b). The ice accretion rates were modeled with the icing standard using the wind speed data from the wind tunnel and the measured LWC and MVD values [8]. The values used in modeling based on the wind tunnel conditions: air density and the absolute viscosity 1.316 kg/m^3 and $1.69 \cdot 10^{-5}$ kg/(m $\cdot$ s) in -5 °C and 1.367 kg/m^3 and $1.64 \cdot 10^{-5}$ kg/(m $\cdot$ s) in -15 °C. The water density in both temperatures was 1000 kg/m^3. The icing rates (mg/s) from the rotating cylinder measurements were calculated from the accumulated total ice mass. The weighed ice load masses were between 3.7 g and 20.0 g.

In Fig. 7 (a) it can be seen that the calculated LWC values without the ice crystal filtering enabled were higher in every measurement and they were vastly overestimated in #3–7. This was most likely caused by the large amount of ice crystals in the -15 °C temperature. When randomly shaped ice crystals are assumed to be spherical, their volume and mass will be largely overestimated. The LWC values where the ice crystals had been removed were closer to the targeted values. In theory, the measured LWC values should be smaller than the inputted water amount to the tunnel would predict if a part of the droplets turned into ice crystals.

The change in the wind speed and targeting the same LWC level requires adjusting of the water flow in the tunnel. This is the most probable explanation for the slight differences in the measured LWC values when comparing

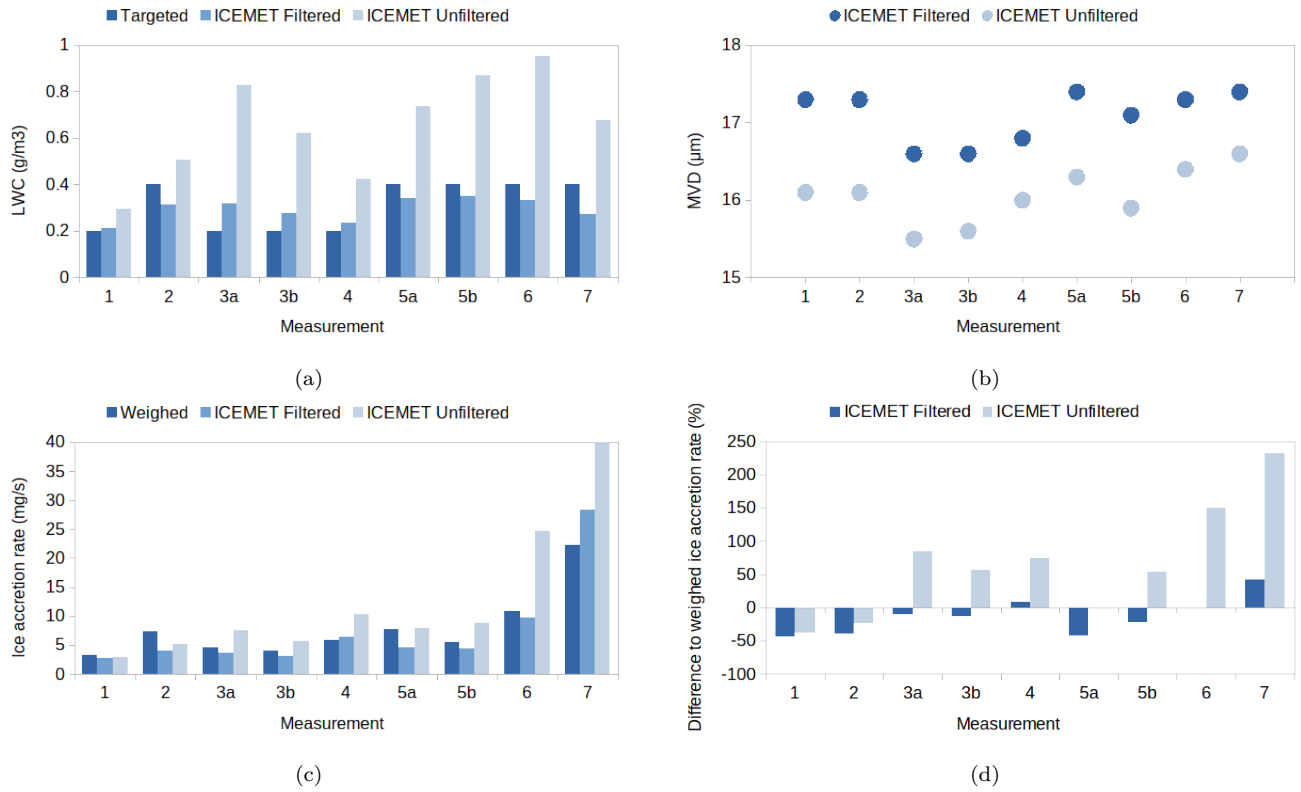

Fig. 7. Wind tunnel results. (a) LWC values targeted by VTT operators and values measured with the ICEMET-sensor with and without circularity filtering. (b) MVD values with and without filtering. (c) Weighed and calculated ice accretion rates. #7 unfiltered. value is 66.4 mg/s. (d) The percentage difference compared to the weighed accretion rate.

results from #3a–b with #4 and #5a–b with #6 and #7.

The MVD values are presented in Fig. 7 (b). The values were approximately 16.5–17.5 µm for the filtered and 15.5–16.5 µm for the unfiltered measurements. This indicates that the filtering reduced more the number of small particles than larger ones.

Ideally the filtering should remove all the ice crystals and leave only droplets for the LWC and MVD calculation. In Fig. 7 (c) it can be seen that for the unfiltered results, the estimated ice accretion rates were all much higher than those measured by the icing standard cylinder. This was expected as the LWC values were higher when the filtering was disabled. A higher wind speed increases the icing rate and thus it caused even a larger overestimation in measurements #6 and #7 between the filtered and unfiltered data.

The percentage difference compared with the weighed accretion is shown in Fig. 7 (d). On average, the unfiltered results were 65.6 % higher than the icing rate of the standard cylinder. The worst result was made in the measurement #7 where the estimated rate was 232.0 % higher. The accretion rates with the ice crystal filtering enabled were much closer to the cylinder values and were 13.4 % lower on average. This would suggest that the used f_c threshold was slightly too strict. There is also the possibility that part of the ice accretion was caused by the ice crystals, which is neglected in the icing model used.

B. The Wind Turbine Nacelle

The ICEMET-sensor's data shows a mixed-phase in-cloud icing event in in February 2017. Similarly to the wind tunnel measurements, the sensor's data was analyzed with and without circularity filtering ($f_c > 1.07$). The icing event is presented in Fig. 8.

The LWC values are shown in Fig. 8 (a). Both LWC curves are very similarly shaped. Just as in the wind tunnel measurements, the unfiltered LWC values were higher. The MVD curves in Fig. 8 (b) were also similar. The spikes between 4:00 and 5:00 represent singular ice crystals. This can be deducted from the fact that the spikes do not appear in the filtered curve and the LWC value did not rise simultaneously.

The icing rate in Fig. 8 (c) was modeled using the ISO 12494:2017 standard cylinder formula and converted to the NREL 5 MW reference turbine blade icing rate by multiplying it by 20 [8], [18]. All the weather data was not available at the measurement time, so the wind speed of 7.5 m/s from the turbine model was used. The used air density was 1.316 kg/m^3, absolute viscosity of the air $1.69 \cdot 10^{-5}$ kg/(m · s) and water density 1000 kg/m^3.

The icing rate started rising after 5:00 together with the LWC and MVD values. It has to be noted that the ISO 12494:2017 ice accretion model has major uncertainty when the collision factor η_1 is less than 0.1 [8]. This was the case between 5:00–5:40. As expected, the unfiltered rates were slightly higher than the filtered rates. The final

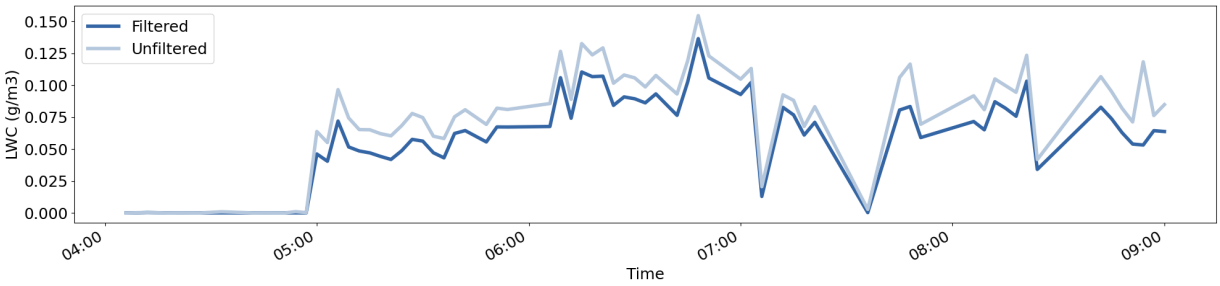

(a) LWC values measured by the ICEMET-sensor.

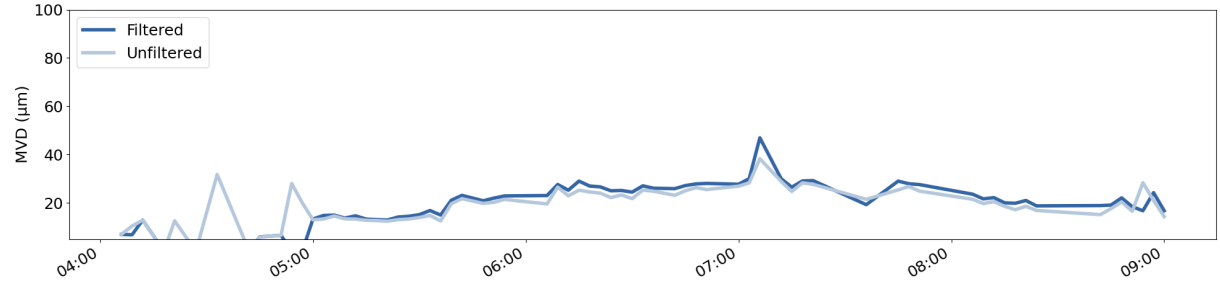

(b) MVD values measured by the ICEMET-sensor.

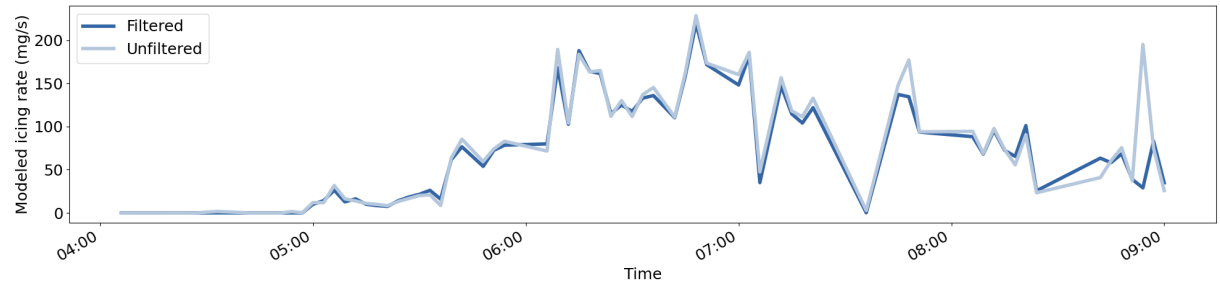

(c) Modeled icing rates on NREL 5 MW reference wind turbine blade per meter.

Fig. 8. Mixed-phase in-cloud wind turbine icing event in February 2017.

accreted ice mass according to the model was 865 g/m for the filtered data and 918 g/m for the unfiltered data. Both masses are quite high and would most likely result in the loss of power production.

IV. Discussion

The LWC and MVD values measured with the ICEMET-sensor can be used together with the ISO 12494:2017 standard's model to estimate ice accretion realistically. The measurements suggest that in order to model icing in the mixed-phase clouds properly, a distinction between droplets and ice crystals must be made. Assuming that all the passing objects are droplets will result in skewed icing rates, especially with high wind speeds.

The wind turbine blade icing model provided a rapid way for estimating ice accretion on the NREL 5 MW reference turbine blade. However, future work is needed both in measurements and modeling to verify if this type of model could be used to estimate ice accretion in actual wind power production during icing events.

Using an imaging droplet sensor offers a good accuracy but also versatility. The filtering of unwanted objects can be done even with basic image analysis and the results can be confirmed by simply looking at the images. Imaging also opens up a possibility for using more sophisticated methods such as machine learning for classifying particles.

The ICEMET-sensor is a novel device that combines a durable ice resistant design with the benefits of holographic imaging. The *in situ* measurements with the sensor can be potentially used to increase the accuracy of the icing models in future.

V. Conclusion

The measurement of mixed-phase cloud icing rate using a novel digital holographic imager and image analysis software was presented. The software has important functionality for separating cloud droplets from other particles such as ice crystals. This offers versatility to examination of mixed-phase icing. The LWC and MVD values measured with the method can be used together with the ISO 12494:2017 icing standard to realistically model ice accretion even in mixed-phase cloud events. This was shown in the presented icing wind tunnel measurements. A simple and unverified case of wind turbine blade ice

accretion modeling was also demonstrated with the droplet data measured in real operating conditions.

References

[1] L. Makkonen, "Models for the growth of rime, glaze, icicles and wet snow on structures," *Philosophical Transactions of the Royal Society of London. Series A: Mathematical, Physical and Engineering Sciences*, vol. 358, no. 1776, pp. 2913–2939, 2000.

[2] O. Parent and A. Ilinca, "Anti-icing and de-icing techniques for wind turbines: Critical review," *Cold regions science and technology*, vol. 65, no. 1, pp. 88–96, 2011.

[3] L. Makkonen, "Analysis of rotating multicylinder data in measuring cloud-droplet size and liquid water content," *Journal of Atmospheric and Oceanic Technology*, vol. 9, no. 3, pp. 258–263, 1992.

[4] S. G. Cober, G. A. Isaac, and J. W. Strapp, "Characterizations of aircraft icing environments that include supercooled large drops," *Journal of Applied Meteorology*, vol. 40, no. 11, pp. 1984–2002, 2001.

[5] K. J. Finstad, E. P. Lozowski, and L. Makkonen, "On the median volume diameter approximation for droplet collision efficiency," *Journal of the atmospheric sciences*, vol. 45, no. 24, pp. 4008–4012, 1988.

[6] L. Makkonen, "Modeling of ice accretion on wires," *Journal of climate and applied meteorology*, vol. 23, no. 6, pp. 929–939, 1984.

[7] A. V. Korolev, G. A. Isaac, and J. Hallett, "Ice particle habits in arctic clouds," *Geophysical research letters*, vol. 26, no. 9, pp. 1299–1302, 1999.

[8] "Atmospheric icing of structures," ISO Standard ISO 12494:2017, Mar. 2017.

[9] D. Baumgardner, H. Jonsson, W. Dawson, D. O'Connor, and R. Newton, "The cloud, aerosol and precipitation spectrometer: a new instrument for cloud investigations," *Atmospheric research*, vol. 59, pp. 251–264, 2001.

[10] S. Lance, C. Brock, D. Rogers, and J. A. Gordon, "Water droplet calibration of the Cloud Droplet Probe (CDP) and in-flight performance in liquid, ice and mixed-phase clouds during ARCPAC," *Atmospheric Measurement Techniques*, vol. 3, no. 6, p. 1683, 2010.

[11] J. P. Fugal, R. A. Shaw, E. W. Saw, and A. V. Sergeyev, "Airborne digital holographic system for cloud particle measurements," *Applied optics*, vol. 43, no. 32, pp. 5987–5995, 2004.

[12] J. Henneberger, J. Fugal, O. Stetzer, and U. Lohmann, "HOLIMO II: a digital holographic instrument for ground-based in situ observations of microphysical properties of mixed-phase clouds," *Atmospheric Measurement Techniques*, vol. 6, pp. 2975–2987, 2013.

[13] S. Rydblom, B. Thörnberg, and E. Olsson, "Field study of LWC and MVD using the droplet imaging instrument," *IEEE Transactions on Instrumentation and Measurement*, vol. 68, no. 2, pp. 614–622, 2018.

[14] V. A. Kaikkonen, E. O. Molkoselkä, and A. J. Mäkynen, "Droplet size distribution and liquid water content monitoring in icing conditions with the ICEMET Sensor," presented at the International Workshops on Atmospheric Icing of Structures, 2019.

[15] V. A. Kaikkonen, E. O. Molkoselkä, and A. J. Mäkynen, "A rotating holographic imager for stationary cloud droplet and ice crystal measurements," *Optical Review*, pp. 1–12, 2020.

[16] S. Rydblom and B. Thörnberg, "Measurement of atmospheric icing and droplets," *IEEE Transactions on Instrumentation and Measurement*, vol. 69, no. 8, pp. 5799–5809, 2020.

[17] E. O. Molkoselkä, V. A. Kaikkonen, and A. J. Mäkynen, "Instrument and method for measuring ice accretion in mixed-phase cloud conditions," in Proc. International Instrumentation and Measurement technology Conference, 2020, p. 33.

[18] V. Turkia, S. Huttunen, and W. Tomas, *Method for estimating wind turbine production losses due to icing*, ser. VTT Technology. Finland: VTT Technical Research Centre of Finland, 2013, no. 114, project code: 72921.

[19] H. J. Juttula, V. A. Kaikkonen, and A. J. Mäkynen, "Study of the aerodynamic sampling effects of a holographic cloud droplet instrument," in Proc. International Instrumentation and Measurement technology Conference, 2020, p. 39.

[20] D. Gabor, "A new microscopic principle," *Nature*, vol. 161, no. 4098, pp. 777–778, 1948.

[21] E. O. Molkoselkä. (2020, Sept.) ICEMET-Server source. [Online]. Available: https://github.com/molkoeero/icemet-server/

[22] G. Bradski, "The OpenCV Library," *Dr. Dobb's Journal of Software Tools*, vol. 25, no. 11, pp. 120–125, Nov. 2000.

[23] J. P. Fugal, T. J. Schulz, and R. A. Shaw, "Practical methods for automated reconstruction and characterization of particles in digital in-line holograms," *Measurement Science and Technology*, vol. 20, no. 7, p. 075501, 2009.

[24] T. Latychevskaia and H.-W. Fink, "Practical algorithms for simulation and reconstruction of digital in-line holograms," *Applied optics*, vol. 54, no. 9, pp. 2424–2434, 2015.

[25] F. C. Groen, I. T. Young, and G. Ligthart, "A comparison of different focus functions for use in autofocus algorithms," *Cytometry: The Journal of the International Society for Analytical Cytology*, vol. 6, no. 2, pp. 81–91, 1985.

[26] Y. Zhang, H. Wang, Y. Wu, M. Tamamitsu, and A. Ozcan, "Edge sparsity criterion for robust holographic autofocusing," *Optics letters*, vol. 42, no. 19, pp. 3824–3827, 2017.

[27] (2020) Local standard deviation of image - MATLAB stdfilt. MathWorks. [Online]. Available: https://www.mathworks.com/help/images/ref/stdfilt.html

[28] T. H. Cormen, C. E. Leiserson, R. L. Rivest, and C. Stein, *Introduction to algorithms*. MIT press, 2009, pp. 414–450.

[29] K. Turkowski, "Filters for common resampling tasks," in *Graphics gems*. Academic Press Professional, Inc., 1990, pp. 147–165.

[30] M. Tiihonen, T. Jokela, L. Makkonen, and G.-J. Bluemink, "VTT icing wind tunnel 2.0," in *Winterwind Presentations 2016*. Umeå, Sweden: Winterwind, Feb 2016.

Eero O. Molkoselkä received the M.Sc. (Tech.) degree in computer science and engineering from the University of Oulu, Oulu, Finland in 2019. He is currently working towards the D.Sc. (Tech.) degree in electrical engineering. His research interests include digital signal processing methods in environmental and industrial measurement applications.

Ville A. Kaikkonen was born in Oulu, Finland. He received the M.Sc. (Tech.) degree in electrical engineering from the University of Oulu, Oulu, Finland, in 2010, where he is currently pursuing the D.Sc. (Tech.) degree in photonics. He has been a Project Researcher with the Measurement Technology research unit, Kajaani, Finland, since 2010. His current research interests include digital holographic imaging.

Anssi J. Mäkynen received the M.Sc. (Tech.) degree (Hons.) and the D.Sc. (Tech.) degree from the University of Oulu, Oulu, Finland, in 1987 and 2000, respectively. He is a Senior Research Fellow and a research group leader in the Faculty of Information Technology and Electrical Engineering, University of Oulu. His current research interests include optical methods for industrial and environmental on-line inspection.